

**The Chandra Deep Field-North Survey:
XVII. Evolution of magnetic activity in old late-type stars¹**

E. D. Feigelson,² A. E. Hornschemeier,^{3,4} G. Micela,⁵ F. E. Bauer,^{2,3,6} D. M. Alexander,^{2,6}
W. N. Brandt,² F. Favata,⁷ S. Sciortino,⁵

and

G. P. Garmire²

ABSTRACT

The extremely sensitive Chandra Deep Field-North (CDF-N) pencil-beam X-ray survey is used to identify and characterize the X-ray emission from old high-latitude main sequence Galactic stars. Our principal goal is to investigate the expected long-term decay of magnetic activity of late-type stars due to the gradual spindown of stellar rotation from a magnetized stellar wind.

Thirteen X-ray sources are associated with late-type stars; 11 of these constitute a well-defined sample for statistical analysis. This sample consists of 2 G, 2 K0–K4, and 7 M2–M5 stars with median V -band magnitude around 19 and median distance around 300 pc. X-ray luminosities are typically $\log L_x \simeq 27$ erg s⁻¹

¹Based in part on observations obtained with the Hobby-Eberly Telescope, which is a joint project of the University of Texas at Austin, the Pennsylvania State University, Stanford University, Ludwig-Maximilians-Universitt München, and Georg-August-Universitt Göttingen.

²Department of Astronomy & Astrophysics, 525 Davey Laboratory, Pennsylvania State University, University Park, PA 16802

³Visiting Astronomer, Kitt Peak National Observatory, National Optical Astronomy Observatory, which is operated by the Association of Universities for Research in Astronomy, Inc. (AURA) under cooperative agreement with the National Science Foundation.

⁴Chandra Fellow, Johns Hopkins University, 3400 N. Charles Street, Baltimore, MD 21218

⁵INAF - Osservatorio Astronomico di Palermo, Piazza del Parlamento 1, 90134 Palermo, Italy

⁶Institute of Astronomy, University of Cambridge, Madingley Road, Cambridge CB3 0HA, United Kingdom

⁷Astrophysics Division, Space Science Department of ESA, ESTEC, Postbus 299, 2200 AG Noordwijk, The Netherlands

but are substantially higher in two cases. The combination of large-amplitude variations on timescales of hours and plasma temperatures around 5 – 30 MK indicates that the observed X-ray emission is dominated by magnetic reconnection flares rather than quiescent coronal emission. These X-ray properties are quantitatively similar to those seen in the active contemporary Sun.

The CDF-N stellar sample is compared to simulations based on convolution of X-ray luminosity functions (XLFs) with the known spatial distribution of old disk stars. The model indicates that the CDF-N stars are the most magnetically active old disk stars. A substantial decline in X-ray luminosities over the $1 < t < 11$ Gyr age interval is required: 39 rather than 11 stars should have been detected if the XLF does not evolve over this time interval. This is the first demonstration that the coronal and flaring components of stellar magnetic activity – and presumably the interior magnetic dynamos responsible for the reconnecting fields at the stellar surface – exhibit long-term decay over the age of the Galactic disk. The model that best fits the magnitudes, spectral types and X-ray luminosities of the sample has $L_x \propto t^{-2}$ erg s⁻¹ which is faster than the t^{-1} decay rate predicted from widely accepted rotational spindown rates and X-ray-activity relations.

Subject headings: stars: activity – stars: coronae – stars: late-type – stars: magnetic fields – X-rays: stars

1. Introduction

It is well-known from studies of young stellar clusters that magnetic activity traced by coronal and flare X-ray emission evolves quickly during the early stages of stellar evolution. During the pre-main sequence phases and upon arrival at the zero-age main sequence (ages $t \sim 10^6 - 10^8$ yr), the X-ray luminosities of low-mass stars typically lie in the range $\log L_x \sim 28 - 30$ erg s⁻¹ and subsequently decay by 2 orders of magnitude over several hundred million years (Micela et al. 1985; Güdel, Guinan, & Skinner 1997; Feigelson & Montmerle 1999; Micela 2002b).

Late-type stellar magnetic activity is regulated principally by rotation in main sequence stars (Pallavicini et al. 1981; Noyes et al. 1984; Baliunas et al. 1995), and its decay with stellar age is attributed to rotational spin-down. While the rotational evolution during the earlier phases of stellar evolution is complex due to magnetic coupling to the circumstellar disk and changing internal structure, the angular momentum behavior is thought to be simpler once the star settles on the main sequence. The only process thought to be important is rotational braking from mass loss where ionized wind particles gain large specific angular momentum

as they travel outward along spiral-shaped magnetic field lines that corotate with the star (Schatzman 1962).

Model calculations indicate that surface rotational velocities should decline as $v_{rot} \propto t^\alpha$ with $-0.75 < \alpha < -0.38$ depending on whether the magnetic field geometry is closer to a dipole or radial configuration (Kawaler 1988) which agrees with empirical findings that $\alpha \simeq -0.5$ (Skumanich 1972). Models considering possible differences in the pre-main sequence disk-locking time, solid body *vs.* differential rotation in the interior, and the onset of magnetic saturation give decay laws over the range $-0.8 < \alpha < -0.2$ for 1–5 Gyr old solar-mass stars (Krishnamurthi et al. 1997). Barnes (2003) argues that the angular momentum loss from the magnetized wind efficiently couples to the entire stellar interior. X-ray coronal and flaring luminosities are well-established tracers of surface magnetic activity, and it is empirically found that $L_x \propto v_{rot}^\beta$ on the main sequence where $\beta \simeq 2$ (Pallavicini et al. 1981; Pizzolato et al. 2003). Combining this with the calculated spin-down relation, the X-ray emission from a typical older main sequence star is expected to decline as

$$L_x \propto t^{\alpha \times \beta} \propto t^{-1} \quad (1)$$

if stars spin-down as $\alpha \simeq -1/2$ and X-ray luminosity scales with rotation as $\beta \simeq 2$.

There have been relatively few empirical measures of this expected decline in magnetic activity in older late-type stars, and most of these involve chromospheric activity. The survey of CaII H and K emission of older solar-mass stars by Soderblom, Duncan, & Johnson (1991) found an activity decay of $R'_{HK} \propto t^{-2/3}$ out to $t \simeq 10$ Gyr. The low-level activity of two slowly rotating analogs of the ancient Sun, β Hyi ($t = 6.7$ Gyr) and 16 Cyg A ($t \sim 9$ Gyr), has been studied in detail (Guinan, Ribas, & Harper 2003). However, other chromospheric studies suggest that the decay of activity may flatten to a constant level after $t \sim 3 - 5$ Gyr and/or that a subpopulation of chromospherically active old stars, possibly from coalesced binaries, is present (Smith & Churchill 1998; Rocha-Pinto, Castilho, & Maciel 2002).

With respect to X-ray emission, even the existence of activity decay between 1 and 10 Gyr has not yet been confidently established. Several dM halo stars observed with the *ROSAT* satellite are systematically fainter ($25.5 < \log L_x < 26.7$ erg s⁻¹) and have cooler ($T \simeq 2-6$ MK) coronal plasmas than in old-disk dM stars ($27.0 < \log L_x < 28.5$ erg s⁻¹, $T > 6$ MK; Micela, Pye & Sciortino 1997). Old-disk stars, in contrast, are found to have *ROSAT* X-ray luminosities and flares similar to the general disk population. Using the *ROSAT* All-Sky Survey dataset and another sample of 24 solar-mass stars with isochronal ages, Micela (2002a) found no clear decay law over the range $1 < t < 10$ Gyr. *ROSAT* All-Sky Survey observations of a large sample of *Hipparcos* F stars showed, contrary to expectations, that X-ray luminosity is correlated (rather than anticorrelated) with increased age inferred from kinematics (Suchkov, Makarov, & Voges 2003). Most studies of the evolution of X-ray

activity indicators use only a rough grouping of stars into logarithmic age intervals (e.g., < 0.01 , $0.1 - 1$, $1 - 10$ Gyr) and thus are unable to address the activity decay expected at later ages.

This issue can be addressed by statistical analyses of deep flux-limited X-ray surveys of random locations rather than shallow all-sky surveys or pointings at known stars. While the stellar X-ray source counts in shallow wide-field X-ray surveys are dominated by the X-ray bright young disk stars, models convolving measured XLFs with Galactic structure predict that older disk stars should dominate the source counts at fainter flux levels (Favata et al. 1992; Micela, Sciortino, & Favata 1993; Sciortino, Favata, & Micela 1995; Guillout et al. 1996; Kuntz, Snowden, & Mushotzky 2001). Even the simple measurement of the total number of stellar sources at faint flux levels can be a sensitive indicator of magnetic activity evolution. At fluxes around 10^{-16} erg cm $^{-2}$ s $^{-1}$ at high Galactic latitudes, stellar soft X-ray source counts are dominated by older ($3 < t < 10$ Gyr) M dwarfs. If the X-ray decay index $\alpha \times \beta \simeq -1$ over $1 < t < 10$ Gyr for these low mass stars, the stellar source counts would be reduced several fold compared to a constant-activity model (see Figure 1 of Kuntz et al.). A handful of individual late-type stars has been found in past deep high-latitude pencil-beam X-ray surveys (e.g., Griffiths et al. 1983; Lehmann et al. 2001; Stern et al. 2002), but these samples have been too small or incomplete for statistical analysis.

Here we address the question of X-ray evolution of older stars with the extremely sensitive *Chandra* Deep Field-North (CDF-N) pencil-beam survey towards $(l, b) = (126, 55)$ which probes the high-galactic latitude X-ray sky to an unprecedented level of 3×10^{-17} cm $^{-2}$ erg s $^{-1}$ in the soft 0.5 – 2 keV band (Alexander et al. 2003). A critically important feature is that optical spectroscopy has been performed for all of the X-ray sources with $V < 22.5$ (Barger et al. 2003). While the great majority of the CDF-N sources are extragalactic (e.g., Hornschemeier et al. 2000; Brandt et al. 2001; Bauer et al. 2002; Alexander et al. 2003), we find that $\simeq 3\%$ are low-mass stars in the outer disk of our Galaxy. Although the sample of 13 stars (11 in our statistical sample) is small, it is the largest well-defined sample of its type and sufficient to provide new constraints on the evolution of X-ray properties over the age of the Galactic disk. We find that the overall stellar XLF must decline over this age range, perhaps even faster than expected with $\alpha \times \beta \simeq -2$ rather than $\simeq -1$ (equation 1), but that hot plasma temperatures and high-amplitude magnetic reconnection flares persists for long times in at least some stars.

Sections 2 – 3 below present the stellar X-ray sample, its X-ray properties, and the associated optical counterparts. Qualitative implications are discussed in §4, and quantitative modelling is presented in §5. Concluding comments appear in §6.

2. *Chandra* observations and analysis

2.1. The CDF-N survey and resulting stellar sample

The X-ray data utilized here are part of the 2 Ms CDF-N survey obtained with the Advanced CCD Imaging Spectrometer (ACIS) detector on board the *Chandra X-ray Observatory*. The satellite and detector are described by Weisskopf et al. (2002). Extragalactic results from the CDF-N project are described in other papers in this series. We briefly summarize the observations and data reduction here. The full observation log, areal exposure, reduction details, and source list are given by Alexander et al. (2003).

The data were collected during 20 separate observations with the ACIS imaging array between November 1999 and February 2002 with a total field of view of ≈ 448 arcmin². The effective exposure time ranges up to 1.95 Ms; about half of the field has an effective exposure time exceeding 1 Ms. The data were corrected for charge transfer inefficiency, cleaned of spurious events, and limited to the 0.5 – 8 keV band. The background level is small (< 1 ct pixel⁻¹) even in the region of highest exposure. Unresolved sources were located in the field using a wavelet-based algorithm. This located 503 unresolved X-ray sources over the entire CDF-N field, about 370 of which were previously reported in the 1 Ms CDF-N sample by Brandt et al. (2001). The field was accurately aligned to the FK5 reference frame via radio source counterparts. The median uncertainty of individual source positions is $\simeq 0.3''$, although faint off-axis sources can have individual offsets as large as $\simeq 1''$. The statistical sample of stellar sources discussed below is based on the first 1 Ms source list (Brandt et al. 2001) which had been optically characterized at the time of this study, although the full 2 Ms dataset was available for X-ray analysis.

It is critical for our modelling of the stellar source population to know the sky coverage as a function of X-ray flux limit. We derived this sensitivity curve for the 1 Ms exposure following the 2 Ms survey methods described by Alexander et al. (2003). The differential sensitivity curve was binned into values listed in Table 1. The precision of this curve is not well-established as it is based on a complex wavelet source detection procedure applied to a field with an inhomogeneous exposure map. We estimate that the sensitivity values could be inaccurate by as much as $\pm 30\%$.

We have extracted our sample of X-ray selected stars as follows. Optical counterparts for CDF-N sources were found down to a limit of $V \simeq 27.3$, and spectra for 85 of the 1 Ms sources with $V < 22.5$ were obtained or reported by Barger et al. (2003).¹ Seventy-three of these spectra showed emission lines from active galactic nuclei and/or were associated

¹The spectroscopic coverage is 98% complete. Two sources with $V < 22.5$, CXOHDFN J123706.7+622549

with morphologically extended galaxies with significant redshifts. The remaining 11 optical spectra show photospheric absorption lines at zero redshift characteristic of normal Galactic stars. Some additional spectra of counterparts from the CDF-N 2 Ms sample (Alexander et al. 2003) were also obtained, from which two more star-like spectra were found.

We thus emerge with a well-defined or ‘statistical’ sample of 11 stellar sources from the CDF-N 1 Ms survey, and two additional stellar sources from the 2 Ms survey. Finding charts are shown in Figure 1. These sources are listed in Table 2 with several X-ray properties extracted from the tables of Alexander et al. (2003): the celestial position; counts in the full band (FB , 0.5 – 8 keV), soft band (SB , 0.5 – 2 keV) and hard band (HB , 2 – 8 keV); the band ratio HB/SB ; the 0.5 – 8 keV count rate; and the effective exposure t_{eff} at that location in the image. The first column “B01 #” gives the source identification number from Brandt et al. (2001). Note that, unlike most extragalactic sources, there were often no hard-band events detected.

None of our stars are included in the V - and I -band sample of stellar-like objects found in $\simeq 25$ arcmin² covering the Hubble Deep Field-North and its flanking fields reported by Mendez & Guzman (1998). Most of our stars are brighter than the stars considered in that study.

2.2. X-ray spectra and fluxes

We analyze here the X-ray spectra using the response matrices appropriate for CTI-corrected ACIS data (Townsend et al. 2002) and the XSPEC spectral fitting package (Arnaud 1996). We adopted thermal plasma models of Mewe (1991). No spectrum required significant interstellar absorption, consistent with the low Galactic column density, $N_H = (1.6 \pm 0.4) \times 10^{20}$ cm⁻² (Stark et al. 1992), in the CDF-N direction. Two-temperature models were used when the least-squares solution to one-temperature models gave unsatisfactory χ^2 goodness-of-fit values.

The ACIS spectra for the 13 stellar sources are shown with the best-fit spectral models in Figure 2. Associated spectral parameters are listed in Table 3: plasma energies for the one- or two-temperature model; the reduced χ^2 value and associated degrees of freedom of the fit; and the SB and FB fluxes obtained by integrating the model. The large uncertainties in the temperatures show that a wide range of spectral models can be fit to the data. In a few cases, additional spectral components which are not statistically significant may be

and J123828.4+620903, were missed.

present (see the notes to Table 3).

2.3. X-ray variability

As the arrival time for each X-ray event is recorded to within ~ 3 sec precision, light curves can be constructed. Long-term lightcurves of the background-corrected count rates seen in each CDF-N observation (not shown) show that most of the sources show factors ≥ 2 variability on timescales of months. Such behavior is expected from any type of stellar magnetic activity.

It is of greater interest that examination of the photon arrival times within each exposure showed a number of likely short-term flares. Figure 3 and Table 3 show cases where the statistical significance of a 1-sample Kolmogorov-Smirnov test of the hypothesis of constant emission has a probability $P_{KS} < 0.001$. We have verified the reality of these flares using the Bayesian Block analysis code developed by Scargle (1998). Altogether there are 9 flares in 7 sources ranging in amplitude from factors of ≈ 3 –10. Most of the flares have short durations of ≈ 1 –3 hours, although one source, CXOHDFN J123625.4+621405, shows a longer-term decay of ~ 1 day (Figure 3).

3. Optical and near-infrared data

3.1. Spectroscopy

From the extensive optical spectroscopy campaign conducted for CDF-N X-ray sources, we show in Figure 4 optical spectra for all 13 stars. Twelve of the spectra presented here were obtained with the Marcario Low Resolution Spectrograph (LRS) (Hill et al. 1998) of the Hobby-Eberly Telescope (HET) 9 meter telescope (Ramsey et al. 1998). The queue-scheduled HET observations occurred on multiple evenings between 2000 February 7 and 2002 March 23. A $2''.0$ slit and 300 line mm^{-1} grism/GG385 blocking filter produced spectra from 4400 – 9000 \AA at 17 \AA resolution; data redward of 7700 \AA are suspect because of possible second-order contamination. The exposure time per source ranged from 2–20 min. The seeing was typically $2''.5$ (FWHM). Wavelength calibration was performed using HgCdZn and Ne lamps, and relative flux calibration was based on spectrophotometric standards.

The remaining star, CXOHDFN J123652.9+620726, was observed with the Ritchey Cretien Spectrograph on the KPNO Mayall 4 m telescope on 2002 May 15. The LB1A CCD detector, BL400 158 line mm^{-1} grating, OG530 blocking filter and $1''.8$ slit were used.

This configuration produced spectra from 5300–10000 Å at 14.5 Å resolution. Wavelength calibration was performed using HeNeAr lamps, and relative flux calibration was performed using spectrophotometric standards.

3.2. Photometry

Photometric observations are presented for the stellar sample in Table 4. For objects fainter than ~ 18 mag, $UBVRz'$ magnitudes are obtained from Barger et al. (2003) which was based on the 1 Ms X-ray CDF-N catalog of Brandt et al. (2001).² For brighter objects where the Barger et al. (2003) observations are saturated, we use the V and I -band photometry of Barger et al. (1999) in the inner $9'0 \times 9'0$ of the field, and our own measurements of the Canada-France-Hawaii Telescope UH8K camera V and I -band images obtained by Wilson (2003) which cover $\approx 90\%$ of CDF-N field. The photometry on the UH8K V and I -band images was performed using SEXTRACTOR (Bertin & Arnouts 1996) with the “Best” magnitude criteria, a 2σ detection threshold, and a 25-pixel sigma Gaussian wavelet.

The accuracies of these optical photometric measurements, whose primary purpose was to identify the extragalactic populations in this survey field, are not sufficiently high or well-established for detailed stellar characterization. For example, a cross-calibration of the UH8K and Barger et al. (1999) VI values shows a scatter around 0.3 mag. We thus cannot reliably search for luminosity class or metallicity effects from the optical photometry.

In the near-infrared JHK bands, photometry is obtained for most of our sample from the 2 Micron All-Sky Survey (2MASS; Cutri et al. 2000). In two faint cases, magnitudes are converted from the HK' measurements of Barger et al. (2003) using the conversion $K \simeq HK' - 0.3$ (Barger et al. 1999).

3.3. Reliability of the X-ray/stellar associations

Table 4 gives the positional offsets between the *Chandra* and stellar sources; most of the latter positions are from the 2MASS survey with typical $\pm 0.2''$ uncertainties with respect to the *Hipparcos* reference frame. One source, #341 (CXOHDFN J123748.1+622126), has

²As all of the stellar sources discussed here fall outside the Hubble Deep Field-North and its Flanking Fields (Williams et al. 1996), deep Hubble Space Telescope data were not available when this analysis was made. We also do not use the UBR measurements of Liu et al. (1999), as these were affected by bad weather, nor the U_nGRK_s photometry of Hogg et al. (2000).

an unusually large offset ($1.8''$) which is probably acceptable because the source lies $\sim 10'$ off-axis in the *Chandra* field where the point spread function is broad. We conclude that the identification of these X-ray sources with Galactic stars is highly reliable.

3.4. Derived quantities

Spectroscopic classifications were obtained by visual comparison of the spectra in Figure 4 to low-resolution spectral atlases (Jacoby, Hunter, & Christian 1984; Kirkpatrick, Henry, & McCarthy 1991; Silva & Cornell 1992). The results are reported in Table 5. We also attempted spectral classification from the photometry in Table 4; most classifications were consistent with the spectroscopic classifications, but classification accuracy was lower and inconsistencies were found. Most of these problems are probably due to inaccurate photometric measurements, although the possibility of binarity cannot be excluded.

If we assume that all stars lie on the main sequence and that negligible interstellar absorption is present, distances can be readily estimated. For the majority of the sample that are M stars, we use the tabulations of Bessell (1991) who gives *BVRIJHK* colors, absolute magnitudes M_I and bolometric corrections BC_I for the *I* band where the bulk of the flux emerges. Because the 2MASS *K*-band magnitudes are more accurate than the available *I*-band measurements, we base our distance calculation on *K* with a classification-dependent ($I - K$) correction. Distances for the G and K stars were estimated from *K* magnitudes with classification-dependent ($V - K$) corrections obtained from Bessell (1990) and absolute M_V luminosities given in Table 15.3.1 of Cox (2000).

These distances are then used to convert the time-averaged soft-band X-ray fluxes from Table 3 to soft X-ray luminosities $\log L_{SB}$. Results are tabulated in the final column of Table 5. From systematic uncertainties in spectral typing, photometry and X-ray spectral fitting, we estimate that distances are uncertain by $\pm 30\%$ and \log X-ray luminosities by ± 0.3 (total range). From the X-ray light curves, we know that the instantaneous luminosity of a given star may differ by several fold from the listed time-averaged value.

We have also calculated the X-ray/near-infrared flux ratio for each star, using the 2MASS filter parameters of Cohen et al. (2003). The relation is as follows:

$$\log \frac{f_X}{f_K} = \log f_X + K/2.5 + 6.95 \quad (2)$$

4. Results and comparison with the Sun

We restrict our interpretation to the well-defined and reliable sample of 11 stars from the 1 Ms CDF-N survey with a peak sensitivity around 3×10^{-17} erg cm⁻² s⁻¹ in the soft X-ray band. Here we have two G stars, two K0–K4 stars, and seven M2–M5 stars. Distances range from 50–460 pc with a median around 300 pc (Table 5). Visual magnitudes range from $V = 14 - 22$ with a median around 19 (Table 4). Soft band X-ray luminosities range from $\log L_{SB} = 26$ to nearly 30 erg s⁻¹ with a median around $L_{SB} \simeq 5 \times 10^{27}$ erg s⁻¹. Most stars show plasma components with temperatures $T \sim 2 - 30$ MK, and the majority show flare events with amplitudes around $\log L_{SB,peak} \sim 27.5 - 28.5$ erg s⁻¹ (Table 3).

Nine of the 11 stars have X-ray luminosities in the range $26.1 < \log L_{SB} < 28.1$ erg s⁻¹ which is essentially the range exhibited by the contemporary Sun through its 22-year cycle (Peres et al. 2000). The two most distant stars have higher luminosities, #341 with $\log L_{SB} = 28.8$ and #370 with 29.8 erg s⁻¹. This is consistent with the expected bias between sensitivity and distance for a flux-limited survey. The observed plasma temperatures ranging from 1 – 30 MK are also consistent with the range seen on the Sun from its quiet, maximum, and flaring states.

If one considers the 11 stars as a homogeneous ensemble, then the flare amplitudes and frequencies of old-disk stars in the CDF-N field can be estimated. We detect nine X-ray flares (§2.3) with characteristic peak luminosities $\log L_{SB,peak} \simeq 28$ erg s⁻¹, and one approaching 30 erg s⁻¹, in a total exposure of $\simeq 22$ Ms. This gives an estimated flare frequency of one flare every $\simeq 2.4$ Ms above $\simeq 10^{28}$ erg s⁻¹. This is similar to the rate of high-X-ray-luminosity flares on the Sun: from several years of *GOES* satellite data, Sammis, Tang, & Zirin (2000) find $\simeq 20$ solar flares with $28.0 \leq \log L_{FB}(peak) \leq 29.0$ erg s⁻¹ in the 1.6 – 12 keV band (close to the *Chandra* full band) or about 1 flare every $\simeq 1.5$ Ms.

We thus find that the flare amplitudes, frequencies and temperatures of the CDF-N old disk stars (most of which are lower mass K- and M-stars) are remarkably similar to the strongest flares seen in the contemporary Sun. This result differs from that reported in *ROSAT* studies of nearby old disk and halo M dwarfs. These show weaker emission around $L_{SB} \sim 2 \times 10^{26}$ erg s⁻¹ and unusually soft emission (Hawley & Feigelson 1994; Micela, Pye, & Sciortino 1997). This is not necessarily a contradiction. The characteristics of the nearby sample, containing well-known high-proper motion stars such as Kapteyn’s star and Barnard’s star, can be roughly viewed as a volume-limited sample representative of average older stars independent of their X-ray luminosities. Our CDF-N sample, in contrast, is a flux-limited X-ray survey capturing only stars at the top of the stellar XLF. Also, our older thin-disk stars may be generally younger than the nearby sample which contains stars kinematically classified as thick disk and halo stars. We thus infer that, while our

sample resembles the contemporary Sun, the average old-disk star probably has weaker X-ray emission and magnetic activity.

5. The decay of stellar X-ray emission

In order to make inferences about the evolution of magnetic activity from these findings, it would be valuable to determine individual ages for the stars in our sample. Unfortunately, this is difficult to achieve. The stars are not sufficiently high above the Galactic plane to be likely members of the thick disk or halo which are known to be ancient ($t \simeq 10 - 13$ Gyr) (Majewski 1993). While the maximum age of stars in the thin disk is 11 ± 1 Gyr (Binney, Dehnen, & Bertelli 2000), we expect a strong age (and thus mass) gradient with height z above the Galactic plane because of the gradual stochastic scattering of stars to orbits reaching several hundred parsecs above the plane. The scattering is also strongly dependent on mass, producing the long-known link between spectral type and exponential scale height. For a typical partitioning of star counts into thin disk, thick disk and halo components, the mass-averaged stellar age rises from $t < 0.5$ Gyr for $z < 100$ pc to $\langle t \rangle \simeq 2$ Gyr at $z = 150$ pc, $\langle t \rangle \simeq 4$ Gyr at $z = 200$ pc, and $5 - 11$ Gyr for $z > 300$ pc (Rocha-Pinto et al. 2000; Robin et al. 2003, H. Rocha-Pinto, 2003 private communication). From these broad distributions, we conclude that the CDF-N stars most likely have ages in the range $3 < t < 11$ Gyr, but that individual ages can not be estimated.³

In the absence of individual stellar age estimates permitting a direct plot of X-ray emission *vs.* age, we compare the observed distribution of CDF-N stars to those predicted by simulated populations assuming different magnetic activity decay laws, $L_x \propto t^{\alpha \times \beta}$, as presented in §1. This approach is feasible only because the CDF-N survey is complete both in its X-ray source population and in the identification of its stellar counterparts, within well-defined flux limits (§2-3). We implement this strategy using the *XCOUNT* model developed by Favata et al. (1992) and Micela, Sciortino, & Favata (1993) which convolves evolving stellar XLFs with the spatial distribution of stars in the Galaxy along a chosen line of sight. *XCOUNT* gives predictions of the magnitudes, spectral types, distances and X-ray luminosities of stars detected in a flux-limited X-ray observation at a chosen Galactic location (l, b). Except for the time dependency of the XLF of interest, there are no free parameters in the model. Even though our sample is small, comparing the CDF-N results with model

³Star #157 may be an exception; at $d \simeq 50$ pc ($z \simeq 40$ pc), its location suggests it may be a young disk star with age $t < 0.5$ Gyr. However, it has the lowest X-ray luminosity of the sample and thus does not exhibit the enhanced magnetic activity of younger stars. We thus suspect it is an old disk star like the others in the CDF-N sample.

predictions can be powerful: any discrepancy in the X-ray flux, spectral type or magnitude distribution can falsify a model calculation and lead to insights into the evolution of stellar X-ray emission in the $1 < t < 11$ Gyr age range.

5.1. Description of the *XCOUNT* model

The version of *XCOUNT* utilized here includes only a thin exponential disk following the Galactic model of Bahcall & Soneira (1980) as revised by Gould, Bahcall, & Flynn (1997). The scale heights are also a function of stellar age: for GKM-type stars, we set $h = 120, 200, 400$ pc for ages $0.01 - 0.1, 0.1 - 1, \text{ and } > 1$ Gyr, respectively. This age dependence has little effect on optical star counts but is very important for X-ray counts at low Galactic latitudes because young stars are much brighter than older stars (Micela, Sciortino, & Favata 1993). Giants are omitted from the *XCOUNT* calculation here because their typical X-ray emissivity is $-6 < \log L_x/L_{bol} < -5$ (Pizzolato, Maggio, & Sciortino 2000) so that only giants with $V \leq 13$ could be detected in the CDF-N survey, none of which are present in the field. Close binary systems, which may be X-ray luminous either by enhanced magnetic activity or accretion, are also omitted due to their rarity. The *XCOUNT* model includes a spatial model for interstellar matter, responsible for absorption both in X-ray and visual bands, but this has no importance for our high-latitude study here. The Besançon model of Robin et al. (2003) gives a similar number and distribution of stars within $d \simeq 600$ pc, but also includes a large number of thick-disk and halo stars extending out many kiloparsecs.⁴ Their omission from the *XCOUNT* simulations should not impact the simulation here because such distant stars would be detected in the CDF-N survey only if their X-ray luminosities greatly exceeded the magnetic activity saturation limit $\log L_t/L_{bol} \sim -3$ of late-type stars (e.g. Vilhu & Walter 1987).

In the standard settings of the *XCOUNT* model, the XLFs are set as follows: the youngest stars with ages $0.01 - 0.1$ Gyr are assigned the *ROSAT* XLF of Pleiades stars (Micela et al. 1996); somewhat older stars with ages $0.1 - 1$ Gyr are assigned the *ROSAT* XLF of the Hyades (Stern, Schmitt, & Kahabka 1995); and stars older than 1 Gyr are assigned the XLF of *Einstein* studies of nearby old-disk stars (Schmitt et al. 1985; Maggio et al. 1987; Barbera et al. 1993). This standard model thus has no magnetic activity decay during the $1 < t < 11$ Gyr age range of interest here. X-ray decay laws were implemented in 1 Gyr bins starting with the Hyades XLF and decreasing the individual X-ray luminosities

⁴This is based on a simulation of the Besançon model produced interactively at www.obs-besancon.fr/modele/model2003.html.

by the factor $t^{\alpha \times \beta}$. Stellar ages t were randomly selected from a multi-exponential disk assuming scale heights $h = 150$ pc for 1 – 2 Gyr stars, $h = 200$ pc for 2 – 5 Gyr stars, and $h = 300$ pc for 5 – 10 Gyr stars (Rocha-Pinto et al. 2000). Trials were made for two decay laws: $\alpha \times \beta = -1$ as expected from past studies (§1) and a faster decay law with $\alpha \times \beta = -2$.

The *XCOUNT* model was then applied to give a simulated stellar population with distances and X-ray luminosities in the direction of the CDF-N survey, $(l, b) = (126, 55)$. We then exclude stars with X-ray fluxes below the CDF-N sensitivity limit given in Table 1 and with *V*-band magnitudes below the optical spectroscopic limit of $V = 22.5$ (§3.1). These two criteria effectively reproduce the sensitivity limits of our study.

5.2. Model results

The results of the *XCOUNT* simulation are shown in Figure 5. The top histograms (thin solid lines) show the underlying disk population in the CDF-N field of view with $V < 22.5$. There are about 91 stars, mostly early M-type which, in the standard model with no XLF evolution for ages $t > 1$ Gyr, have mostly low X-ray luminosities in the range $26 < \log L_x < 28$ erg s⁻¹. The next histogram (dot-dashed line) shows that 39 of the 90 stars would be detected with the CDF-N X-ray sensitivity curve (Table 1) in the standard no-evolution model. The detected stars would include most of the G- and K-type stars but less than half of the M stars. As expected in a flux-limited survey, the X-ray detected sample would be biased toward the high- L_x end of the underlying XLF.

The prediction of 39 detections from the standard *XCOUNT* model with no late XLF evolution is clearly much higher than the observed X-ray selected population of 11 stars. To determine whether this is a significant difference, we attempt to evaluate the sources of uncertainty in the observed numbers. On the observational side, there is a systematic uncertainty in the CDF-N areal coverage *vs.* sensitivity curve (§2.1) and a statistical uncertainty in the 11-star sample. The areal coverage has a plausible range of $\pm 30\%$ arising primarily from the ill-determined sensitivity of the wavelet source detection across the ACIS field. The 90% Poisson confidence interval for 11 observed stars is 7 – 16 stars. On the modelling side, there are systematic uncertainties in the Galactic structure model and adopted XLFs, as well as statistical \sqrt{N} uncertainties in the *XCOUNT* simulation. We estimate a 90% range of $\pm 30\%$ for these uncertainties. A rough combination of these statistical and systematic sources of uncertainties gives an estimated range of 80 – 100%, or an approximate 90% confidence interval of 5 – 22 stars.

We thus conclude that the prediction of 39 stars from the model without $t > 1$ Gyr

magnetic activity evolution is confidently falsified. The dashed histograms in Figure 5 show that the rapid-evolution model where $\alpha \times \beta = -2$ in the relation $L_x \propto t^{\alpha \times \beta}$ matches the observed distributions very well. It predicts 14 X-ray detected stars, consistent with the observed 11 stars. The predicted distributions of apparent magnitude, spectral type and X-ray luminosity (and, implicitly, stellar distances) are almost identical to the observed distributions. The $\alpha \times \beta = -1$ model predictions lie between the no-evolution $\alpha \times \beta = 0$ and rapid-evolution $\alpha \times \beta = -2$ models. It overpredicts the X-ray sample size and gives a poor match to the spectral type and X-ray luminosity distributions, but it is not definitely inconsistent with the observations given the estimated uncertainties.

6. Discussion

6.1. The detected stellar population

We present the first quantitative study of stellar sources in a deep X-ray pencil-beam high-latitude survey designed to investigate the evolution of coronal and flare magnetic activity in older late-type stars. It is based on the extremely deep *Chandra* image of the *Chandra* Deep Field-North field with optical photometry and spectroscopy of all X-ray sources down to $V = 22.5$. From the 1 Ms exposure, we find 11 stars which constitute our statistical sample. Two additional X-ray stars are identified in the 2 Ms exposure.

The 11 stars consist of two G, two K and seven M stars with photometric distances ranging from 50 – 510 pc, assuming they lie on the main sequence. At these distances, luminosities fall in the range $26.1 < \log L_x < 29.8$ erg s⁻¹ (0.5 – 8 keV band) and are consistent with those seen in the integrated field population of nearby disk stars (Schmitt 1997). The luminosities, temperatures and flaring amplitudes and frequencies of the CDF-N stars are also remarkably similar to those of the contemporary Sun (§4).

Comparing the observed stars to the expected Galactic population along the CDF-N line of sight, we infer that the stars are mostly dwarfs of the old-disk population with characteristic ages in the $3 < t < 11$ Gyr range (§5). The CDF-N observation is insufficiently sensitive to detect the thick-disk or halo populations, and the field is too small to contain more than 0 – 1 young ($t < 1$ Gyr) thin disk stars. We thus provide here an empirical demonstration that stellar coronae and flares – and presumably the interior magnetic dynamos responsible for the reconnecting fields at the stellar surface – persist over the age of the Galactic disk. However, the detected sample comprises only the most X-ray-luminous $\simeq 10\%$ within the old-disk population. The typical old-disk stars probably have X-ray luminosities considerably below the median value $L_{SB} \simeq 5 \times 10^{27}$ erg s⁻¹ of our sample.

6.2. Magnetic activity decay on the main sequence

Quantitative modelling of the CDF-N sample, including the spectral types, distances and X-ray luminosities, clearly requires substantial decline in X-ray luminosities over the $1 < t < 11$ Gyr age interval. This is the first empirical demonstration of the long-term decay of the coronal and flaring components of magnetic activity. An excellent fit to the sample is obtained with $\log L_x \propto t^{\alpha \times \beta} \text{ erg s}^{-1}$ with an $\alpha \times \beta = -2$ decay law (§5.2, Figure 5). However, due to the small sample and systematic uncertainties, we cannot confidently exclude the $\alpha \times \beta = -1$ decay law which is expected from a simple application of $L_x \propto v_{rot}^\beta$ with $\beta = 2$ X-ray activity-rotation relation and a $v_{rot} \propto t^\alpha$ rotation-age relation with $\alpha = -1/2$ (§1).

If the $\alpha \times \beta = -2$ result is confirmed to be correct by future studies (§7), we will face the challenge of explaining why the decay of magnetic activity is much faster than the expected value $\alpha \times \beta = -1$. One class of explanations is that the rotational spindown for older disk stars is more rapid than the $\alpha = -1/2$ rate expected from constant magnetized stellar winds (Kawaler 1988). It is possible that the coupling efficiency between outer and inner layers of the stars weakens with age, or that it is mass-dependent (see discussion in Barnes 2003). Alternatively, the Sun’s wind strength may be lower than in these magnetically active old disk stars, or coronal mass ejections may contribute significantly to stellar angular deceleration.

The alternative class of explanations is that the magnetic activity-rotation relation steepens with age so that $\beta \simeq 4$. Perhaps magnetic field generation at the tachocline becomes more efficient as the stars age and their convective zone thicken. Coronal densities and volumes may scale differently with rotation as stars age (see discussion in Ivanova & Taam 2003).

6.3. Flaring in old stars

The extremely long CDF-N exposures give us unprecedented ability to study the temporal behavior and spectra of X-ray emission from older stars. We see high-amplitude flares with $L_{x,peak} \sim 10^{27} \text{ erg s}^{-1}$ (and in one case, $L_{x,peak} \sim 10^{30} \text{ erg s}^{-1}$) in half of the 11 CDF-N stars (§2.3). This is a good indication that magnetic dynamos, likely solar-type $\alpha - \Omega$ dynamos arising from differential rotation at the radiative-convective zone interface, are responsible for the X-ray emission. Our results do not support a view where only a quiescent basal chromosphere (e.g., Buchholz, Ulmschneider, & Cuntz 1998) persists in all older main sequence stars. At least in the 10% most active stars in the $3 < t < 11$ Gyr range, solar-type flaring is common.

The presence of stellar flares in old disk stars also provides new empirical information

relevant to the enigmatic star-to-star variations in lithium abundances in old-disk and halo stars (Spite & Spite 1982). While several models for the lithium inhomogeneities have been considered, one possibility is that the lithium is produced by spallation in magnetic reconnection flares (Ryter et al. 1970; Montes & Ramsey 1998).

7. Avenues for future research

High-resolution spectroscopic study of the 11 X-ray-selected CDF-N stars would yield important insights into the magnetic activity of older stars. Measurement of surface rotational velocities $v \sin i$ would allow direct measurement of β , the X-ray activity-rotation relation. Measurement of low metallicities and/or high radial velocities might reveal that some stars are members of the ancient thick-disk or halo populations. For the G and K stars with significant B -band flux, measurement of the chromospheric indicator $\log R'_{HK}$ would permit comparison of chromospheric and coronal/flare magnetic activity. Measurement of a strong Li $\lambda 6707$ line might test lithium spallation models. Obtaining sufficiently high-signal and high-resolution spectra on such faint stars is a significant observational challenge.

A clear limitation of the present study is its small 11-star sample. One consequence of this small sample is our confluence of dwarf G, K and M stars to estimate a single magnetic activity decay rate, while it is quite possible that the magnetic evolution is mass dependent. If the sample of X-ray-selected old-disk stars could be increased several fold, then considerably more powerful constraints on the evolution of magnetic activity would emerge. The demographic approach based on star counts in deep X-ray pencil-beam surveys, can be extended in three ways. First, the CDF-N itself can be investigated at a deeper flux level using the full 2 Ms observation, lower signal-to-noise sources, and stacking techniques to obtain sample-averaged X-ray emission of previously identified stars in the field. The *Chandra* Deep Field-South offers a similar opportunity.⁵ Proper motions derived from multi-epoch optical observations of the GOODS survey regions may also give valuable constraints on the kinematics of X-ray selected high-latitude stars.

Second, while our count rates indicate that *Chandra* observations at high Galactic latitude with exposure ≤ 0.3 Ms will give a low return on stellar sources, such shorter

⁵The *Chandra* Deep Field-South catalog of Giacconi et al. (2002) has several sources with soft spectra and relatively bright optical counterparts which are good candidates for older Galactic stars. The brightest cases are CXOCDFS J033249.8-275455 (K0 V, $V = 16.16$, $U - B = 0.29$, $B - V = 0.50$, $V - R = 0.56$, $V - I = 1.01$, $J = 14.62$, $K = 21.03$; Groenewegen et al. 2002) and CXOCDFS J033242.1-275704 ($V = 14.00$, $B - V = 2.00$; Wolf et al. 2001).

exposures at intermediate latitudes which intersect greater column densities of old disk stars may be successful. For example, two Galactic dwarfs are found among 153 sources in the 0.18 Ms Lynx field at $b = 39^\circ$ (Stern et al. 2002). Large-scale spectroscopic studies of serendipitous X-ray sources, such as the *Chandra* Multiwavelength Project (Green et al. 2004) and *XMM – Newton* Serendipitous Sky Survey (Watson 2003), could produce quite rich stellar samples. Intermediate- and high-latitude surveys with the EPIC imaging CCD on the *XMM – Newton* satellite are particularly promising, given the detector’s larger field of view compared to *Chandra*. One coronal star has been found among the first 27 *XMM – Newton* sources studied in the medium-sensitivity high-latitude *AXIS* survey (Barcons et al. 2002). We thus look forward to both *Chandra* and *XMM – Newton* studies to substantially extend the present study of the late evolution of stellar magnetic activity.

Acknowledgments The first three authors contributed equally to this study. Pat Broos and Leisa Townsley (Penn State) played critical roles in developing data analysis techniques, Gillian Wilson (Hawaii) kindly provided access to unpublished optical images, and Helio Rocha-Pinto and Steve Majewski (Virginia) provided helpful advice on Galactic structure. The anonymous referee gave a thoughtful and useful commentary on the manuscript. The Marcario Low Resolution Spectrograph is named for Mike Marcario of High Lonesome Optics who fabricated several optics for the instrument but died before its completion. The LRS is a joint project of the Hobby-Eberly Telescope partnership (the University of Texas at Austin, the Pennsylvania State University, Stanford University, Ludwig-Maximilians-Universität München, and Georg-August-Universität Göttingen) and the Instituto de Astronomía de la Universidad Nacional Autónoma de México. The HET is named in honor of its principal benefactors, William P. Hobby and Robert E. Eberly. We gratefully acknowledge the financial support of NASA grant NAS 8-38252 (GPG, PI), NASA GSRP grant NGT5-50247 and *Chandra* Fellowship PF2-30021 (AEH), CXC grant GO2-3187A and NSF CAREER Award AST 9983783 (FEB, DMA, WNB). GM and SS acknowledge financial support from ASI contracts and MIUR PRIN grants.

REFERENCES

- Alexander, D. M., et al. 2003, ApJ, AJ, 126, 539
- Arnaud, K. A. 1996, in Data Analysis Software and Systems V, ed. G. H. Jacoby & J. Barnes (San Francisco:ASP), 17
- Bahcall, J. N. & Soneira, R. M. 1980, ApJS, 44, 73
- Baliunas, S. L. et al. 1995, ApJ, 438, 269
- Barbera, M., Micela, G., Sciortino, S., Harnden, F. R., & Rosner, R. 1993, ApJ, 414, 846
- Barcons, X. et al. 2002, A&A, 382, 522
- Barger, A. J., Cowie, L. L., Trentham, N., Fulton, E., Hu, E. M., Songaila, A., & Hall, D. 1999, AJ, 117, 102
- Barger, A. J., Cowie, L. L., Brandt, W. N., Capak, P., Garmire, G. P., Hornschemeier, A. E., Steffen, A. T., & Wehner, E. H. 2002, AJ, 124, 1839
- Barnes, S. A. 2003, ApJ, 586, 464
- Bauer, F. E., Alexander, D. M., Brandt, W. N., Hornschemeier, A. E., Vignali, C., Garmire, G. P., & Schneider, D. P. 2002, AJ, 124, 2351
- Bertin, E. & Arnouts, S. 1996, A&AS, 117, 393
- Bessell, M. S. & Brett, J. M. 1988, PASP, 100, 1134
- Bessell, M. S. 1990, PASP, 102, 1181
- Bessell, M. S. 1991, AJ, 101, 662
- Binney, J., Dehnen, W., & Bertelli, G. 2000, MNRAS, 318, 658
- Brandt, W. N. et al. 2001, AJ, 122, 2810
- Buchholz, B., Ulmschneider, P., & Cuntz, M. 1998, ApJ, 494, 700
- Chen, B. et al. 2001, ApJ, 553, 184
- Cohen, M., Wheaton, W. A., & Megeath, S. T. 2003, AJ, in press (astro-ph/0304350)
- Cox, A. N. (ed.) 2000, Allen's astrophysical quantities, 4th ed., New York:AIP Press

- Cutri, R. M. 2000, Explanatory Supplement to the 2MASS Second Incremental Data Release, IPAC/Caltech
- Favata, F., Micela, G., Sciortino, S., & Vaiana, G. S. 1992, *A&A*, 256, 86
- Feigelson, E. D. & Montmerle, T. 1999, *ARA&A*, 37, 363
- Giacconi, R. et al. 2002, *ApJS*, 139, 369
- Gould, A., Bahcall, J. N., & Flynn, C. 1997, *ApJ*, 482, 913
- Green, P. J., et al. 2004, *ApJS*, 150, 43
- Griffiths, R. E. et al. 1983, *ApJ*, 269, 375
- Groenewegen, M. A. T. et al. 2002, *A&A*, 392, 741
- Güdel, M., Guinan, E. F., & Skinner, S. L. 1997, *ApJ*, 483, 947
- Guillout, P., Haywood, M., Motch, C., & Robin, A. C. 1996, *A&A*, 316, 89
- Guinan, E. F., Ribas, I., & Harper, G. M. 2003, *ApJ*, 594, 561
- Hawley, S. L. & Feigelson, E. D. 1994, *ASP Conf. Ser. 64: Cool Stars, Stellar Systems, and the Sun*, 8, 89
- Haywood, M., Robin, A. C., & Creze, M. 1997, *A&A*, 320, 440
- Hill, G. J., Nicklas, H. E., MacQueen, P. J., Mitsch, W., Wellem, W., Altmann, W., Wesley, G. L., & Ray, F. B. 1998, in *Proc. SPIE*, 3355, 433
- Hogg, D. W. et al. 2000, *ApJS*, 127, 1
- Hornschemeier, A. E. et al. 2000, *ApJ*, 541, 49
- Ivanova, N. & Taam, R. E. 2003, *ApJ*, 599, 516
- Jacoby, G. H., Hunter, D. A., & Christian, C. A. 1984, *ApJS*, 56, 257
- Kawaler, S. D. 1988, *ApJ*, 333, 236
- Kirkpatrick, J. D., Henry, T. J., & McCarthy, D. W. 1991, *ApJS*, 77, 417
- Krishnamurthi, A., Pinsonneault, M. H., Barnes, S., & Sofia, S. 1997, *ApJ*, 480, 303
- Kuntz, K. D., Snowden, S. L., & Mushotzky, R. F. 2001, *ApJ*, 548, L119

- Lehmann, I. et al. 2001, *A&A*, 371, 833
- Liu, C. T., Petry, C. E., Impey, C. D., & Foltz, C. B. 1999, *AJ*, 118, 1912
- Maggio, A., Sciortino, S., Vaiana, G. S., Majer, P., Bookbinder, J., Golub, L., Harnden, F. R., & Rosner, R. 1987, *ApJ*, 315, 687
- Majewski, S. R. 1993, *ARA&A*, 31, 575
- Mendez, R. A. & Guzman, R. 1998, *A&A*, 333, 106
- Mewe, R. 1991, *A&A Rev.*, 3, 127
- Micela, G., Sciortino, S., Serio, S., Vaiana, G. S., Bookbinder, J., Golub, L., Harnden, F. R., & Rosner, R. 1985, *ApJ*, 292, 172
- Micela, G., Sciortino, S., & Favata, F. 1993, *ApJ*, 412, 618
- Micela, G., Sciortino, S., Kashyap, V., Harnden, F. R., & Rosner, R. 1996, *ApJS*, 102, 75
- Micela, G., Pye, J., & Sciortino, S. 1997, *A&A*, 320, 865
- Micela, G. 2002a, in *The Evolving Sun and its Influence on Planetary Environments* (B. Montesinos et al., eds.), *ASP Conf.* 269, 107.
- Micela, G. 2002b, in *Stellar Coronae in the Chandra and XMM-Newton Era*, *ASP Conf Ser*, in press
- Montes, D. & Ramsey, L. W. 1998, *A&A*, 340, L5
- Noyes, R. W., Hartmann, L. W., Baliunas, S. L., Duncan, D. K., & Vaughan, A. H. 1984, *ApJ*, 279, 763
- Pallavicini, R., Golub, L., Rosner, R., Vaiana, G. S., Ayres, T., & Linsky, J. L. 1981, *ApJ*, 248, 279
- Peres, G., Orlando, S., Reale, F., Rosner, R., & Hudson, H. 2000, *ApJ*, 528, 537
- Pizzolato, N., Maggio, A., & Sciortino, S. 2000, *A&A*, 361, 614
- Pizzolato, N., Maggio, A., Micela, G., Sciortino, S., & Ventura, P. 2003, *A&A*, 397, 147
- Ramsey, L. W., et al. 1998, in *Proc. SPIE Vol. 3352*, p. 34-42, *Advanced Technology Optical/IR Telescopes VI*, Larry M. Stepp; Ed., Vol. 3352, 34

- Robin, A. C., Reylé, C., Derrière, S., & Picaud, S. 2003, *A&A*, 409, 523
- Rocha-Pinto, H. J., Scalo, J., Maciel, W. J., & Flynn, C. 2000, *A&A*, 358, 869
- Rocha-Pinto, H. J., Castilho, B. V., & Maciel, W. J. 2002, *A&A*, 384, 912
- Ryter, C., Reeves, H., Gradsztajn, E., & Audouze, J. 1970, *A&A*, 8, 389
- Sammis, I., Tang, F., & Zirin, H. 2000, *ApJ*, 540, 583
- Scargle, J. D. 1998, *ApJ*, 504, 405
- Schatzman, E. 1962, *Annales d'Astrophysique*, 25, 18
- Schmitt, J. H. M. M., Golub, L., Harnden, F. R., Maxson, C. W., Rosner, R., & Vaiana, G. S. 1985, *ApJ*, 290, 307
- Schmitt, J. H. M. M. 1997, *A&A*, 318, 215
- Schrijver, C. J. & Zwaan, C. 2000, *Solar and stellar magnetic activity*, New York:Cambridge University Press
- Schuster, W. J. & Nissen, P. E. 1989, *A&A*, 222, 69
- Sciortino, S., Favata, F., & Micela, G. 1995, *A&A*, 296, 370
- Silva, D. R. & Cornell, M. E. 1992, *ApJS*, 81, 865
- Skumanich, A. 1972, *ApJ*, 171, 565
- Smith, G. H. & Churchill, C. W. 1998, *MNRAS*, 297, 388
- Soderblom, D. R., Duncan, D. K., & Johnson, D. R. H. 1991, *ApJ*, 375, 722
- Spite, F. & Spite, M. 1982, *A&A*, 115, 357
- Stark, A. A., Gammie, C. F., Wilson, R. W., Bally, J., Linke, R. A., Heiles, C., & Hurwitz, M. 1992, *ApJS*, 79, 77
- Stauffer, J. R., Caillault, J.-P., Gagne, M., Prosser, C. F., & Hartmann, L. W. 1994, *ApJS*, 91, 625
- Stern, R. A., Schmitt, J. H. M. M., & Kahabka, P. T. 1995, *ApJ*, 448, 683
- Stern, D. et al. 2002, *AJ*, 123, 2223

- Suchkov, A. A., Makarov, V. V., & Voges, W. 2003, *ApJ*, 595, 1206
- Townsley, L. K., Broos, P. S., Nousek, J. A., & Garmire, G. P. 2002, *Nucl. Instr. Methods*, in press (astro-ph/0111031)
- Vilhu, O. & Walter, F. M. 1987, *ApJ*, 321, 958
- Watson, M. 2003, in *Maps of the Cosmos*, IAU Symp. 216, San Francisco:ASP.
- Weisskopf, M. C., Brinkman, B., Canizares, C., Garmire, G., Murray, S., & Van Speybroeck, L. P. 2002, *PASP*, 114, 1
- Williams, R. E. et al. 1996, *AJ*, 112, 1335
- Wilson, G. 2003, *ApJ*, 585, 191
- Wolf, C., Dye, S., Kleinheinrich, M., Meisenheimer, K., Rix, H.-W., & Wisotzki, L. 2001, *A&A*, 377, 442

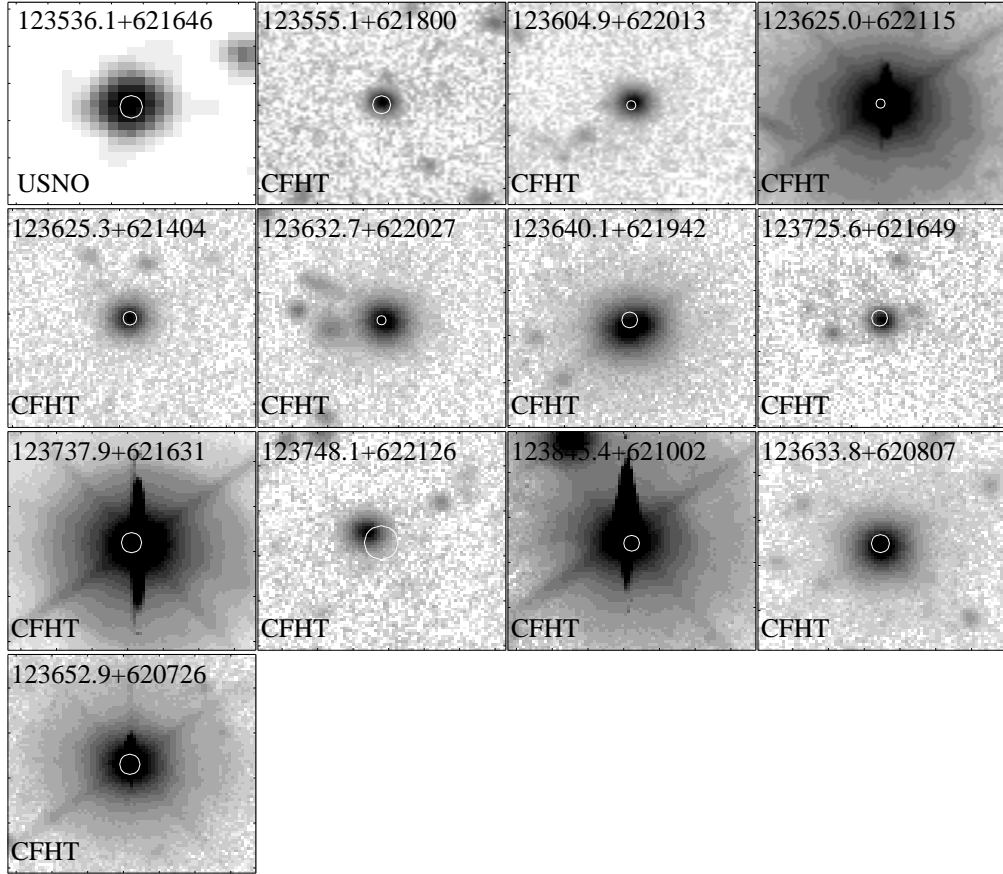


Fig. 1.— Chandra ACIS source positions (white circles) superposed on *I*-band images (kindly provided by G. Wilson), except for the first panel where the Palomar *R*-band sky survey image is shown. Each panel is $25'' \times 25''$ with North above and East to the right. The error circle radii are the X-ray positional errors given in Table 2.

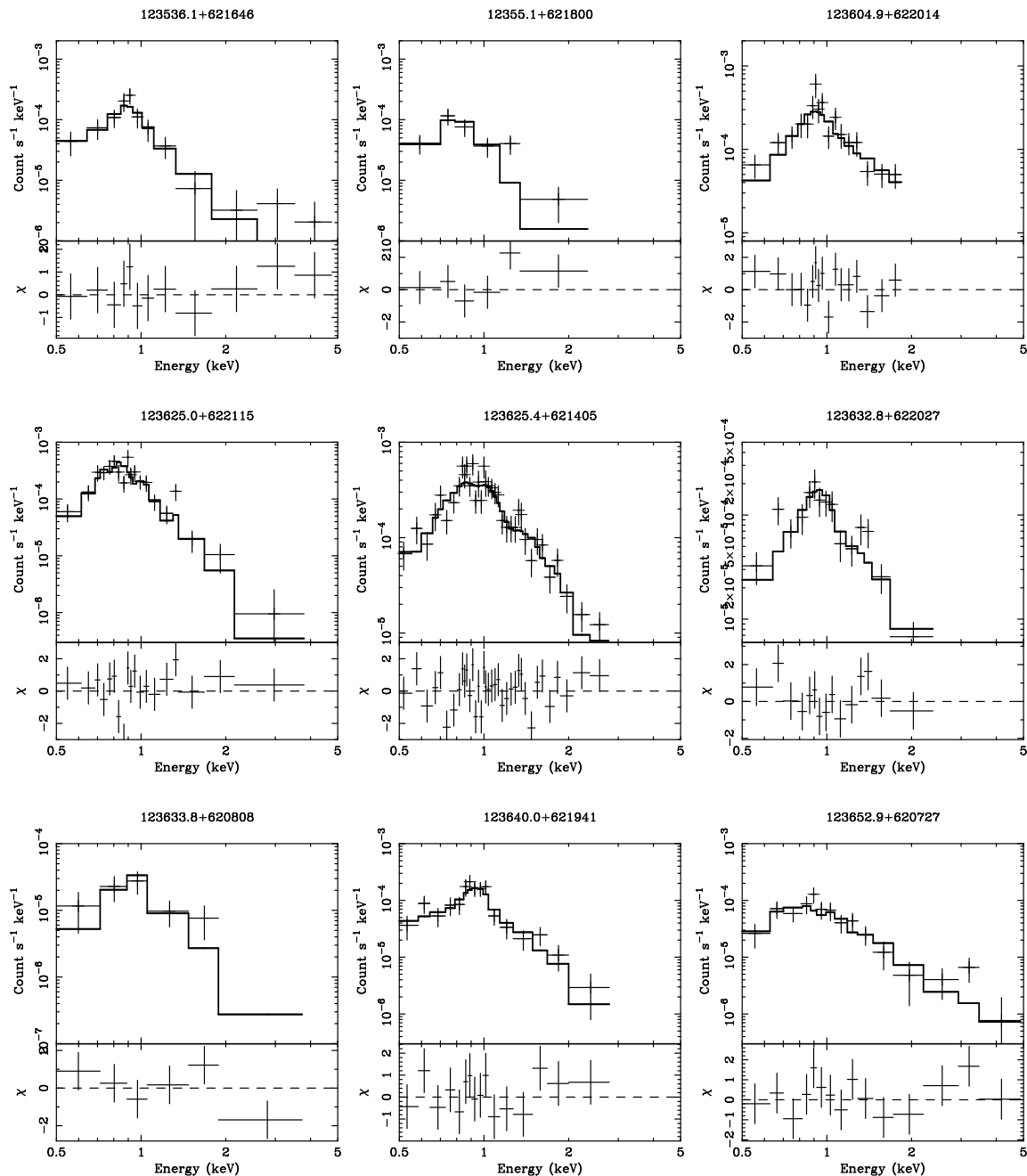
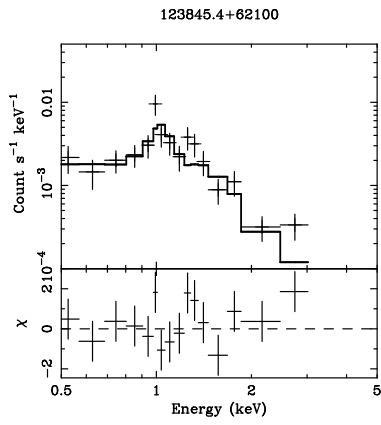
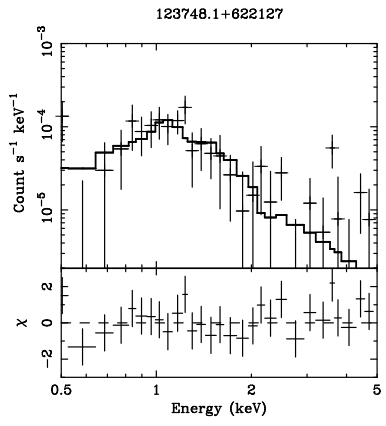
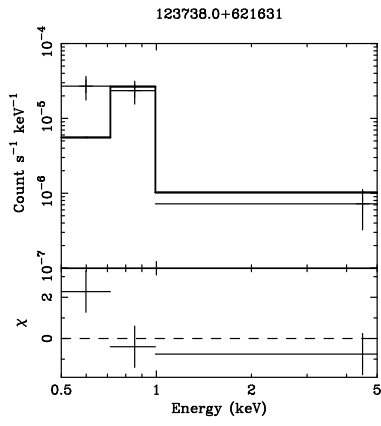
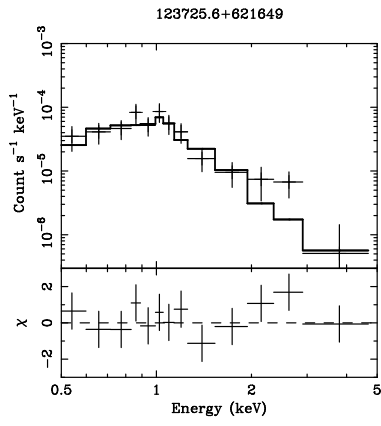


Fig. 2.— ACIS spectra of the 13 CDF-N stars with best-fit plasma models (Table 3) superposed. The lower part of each panel shows the deviation of the data from the model in units of σ .



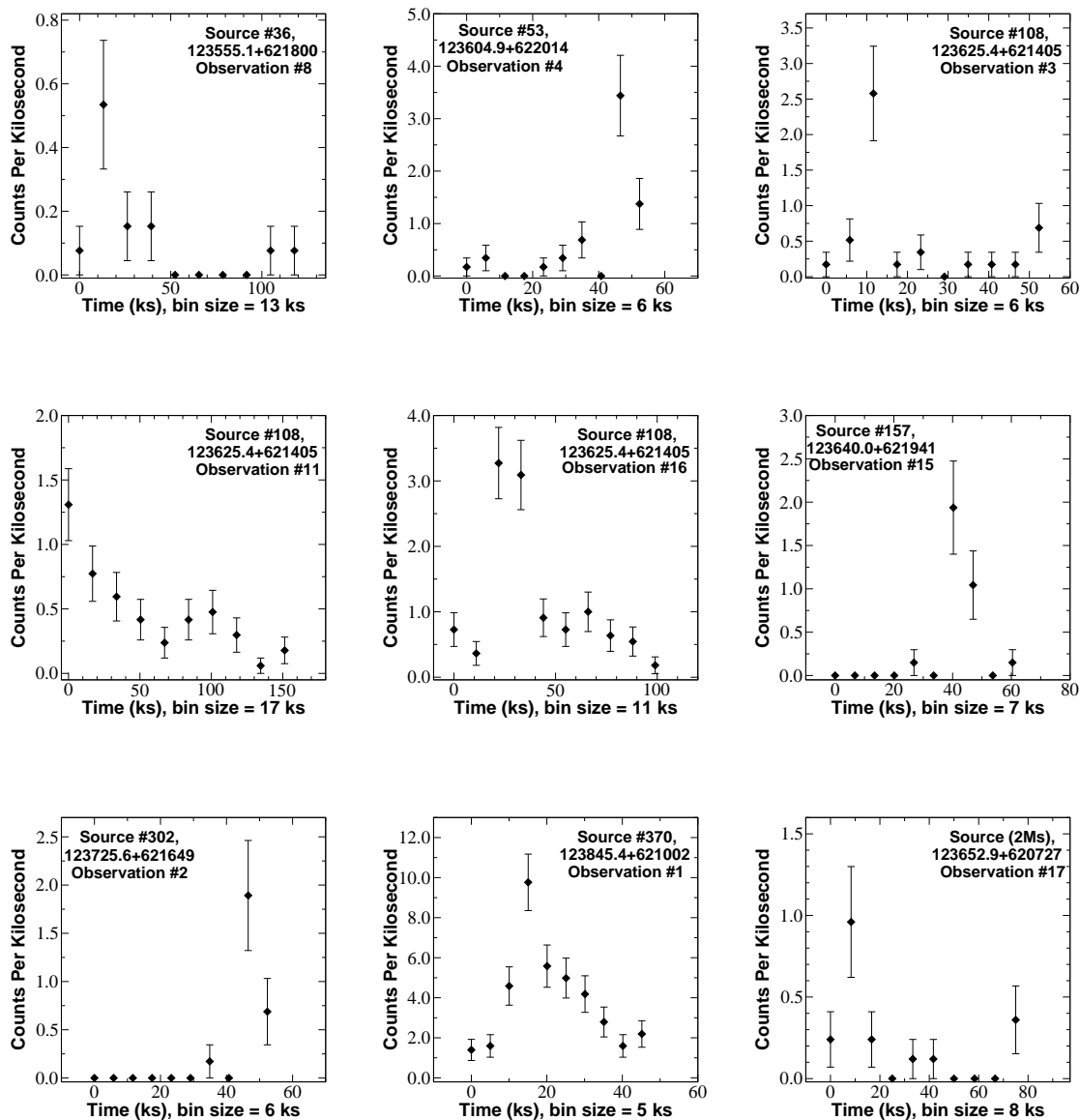


Fig. 3.— Portions of the *Chandra* ACIS lightcurves showing statistically significant short-timescale flares from CDF-N stars. The ordinate gives count rate in cts ks^{-1} and abscissa gives time in ks.

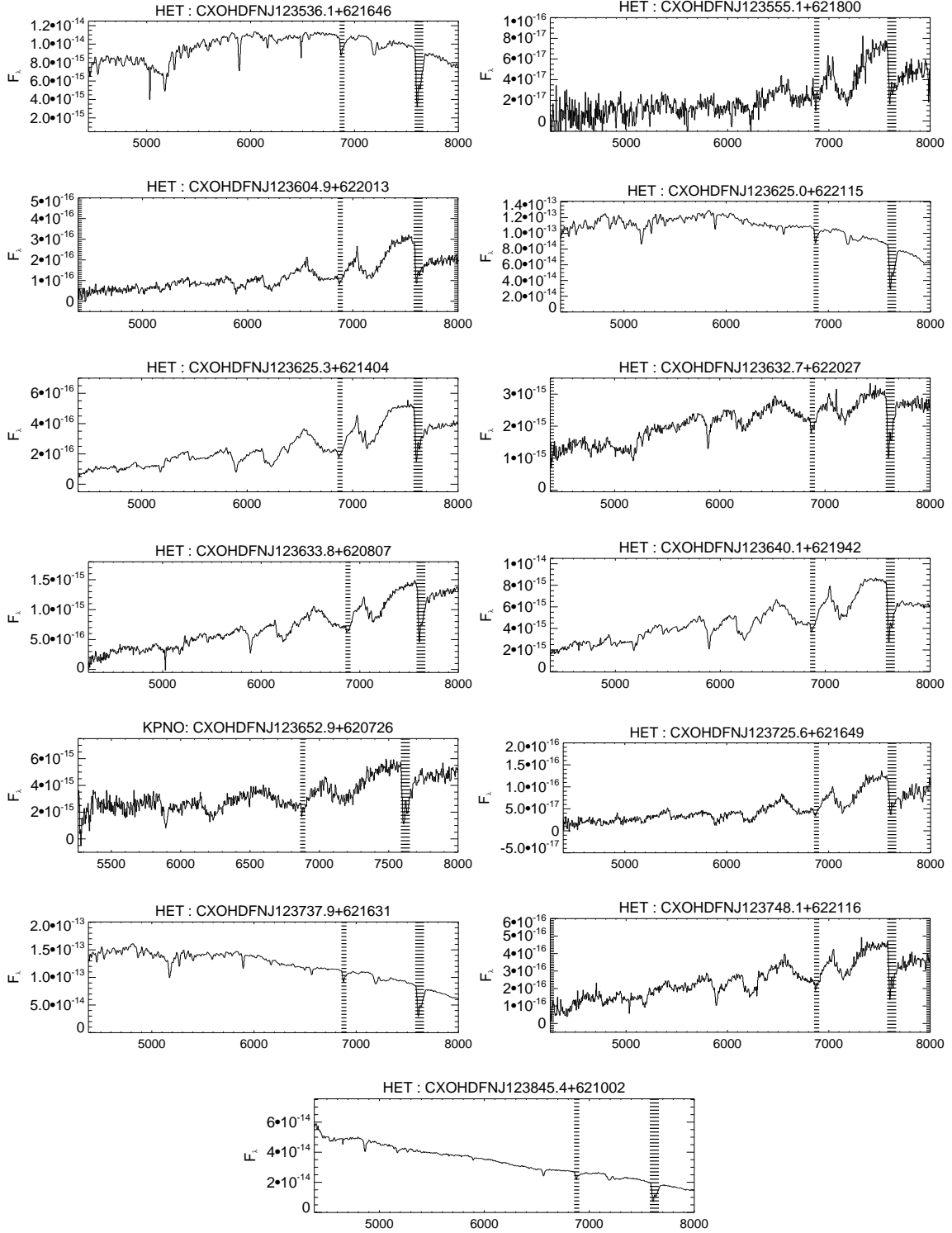


Fig. 4.— Optical spectra of 13 CDF-N stars obtained with the Hobby-Eberly Telescope 9m and Kitt Peak 4m telescopes. The abscissa give wavelength in Angstrom and the ordinates give flux densities in $\text{erg s}^{-1} \text{cm}^{-2} \text{\AA}^{-1}$. Hatched areas denote spectral regions with telluric contamination.

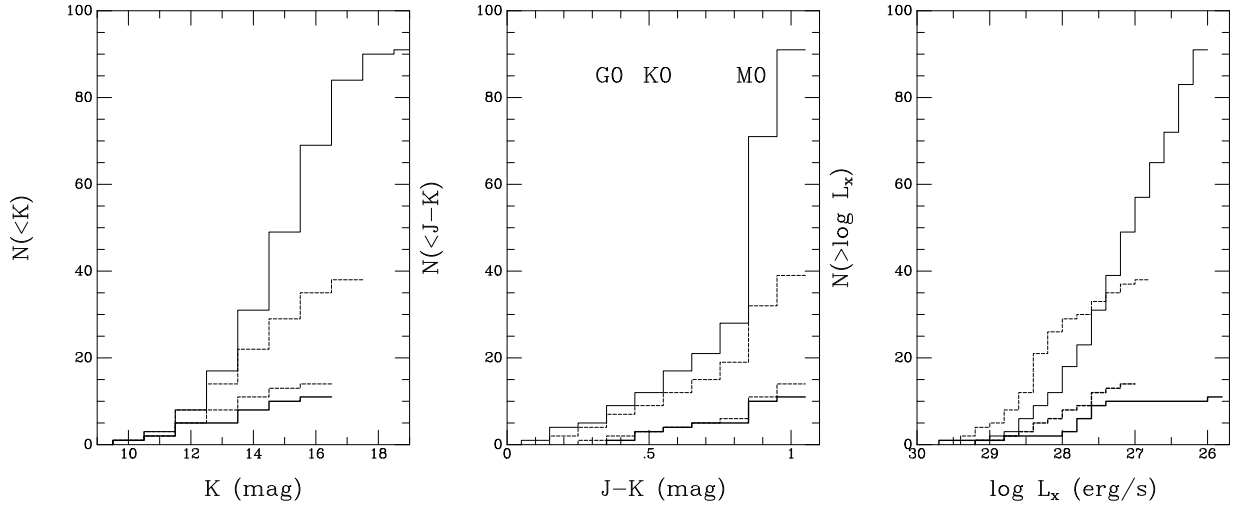


Fig. 5.— Comparison of cumulative distributions of three stellar parameters for *XCOUNT* models of the CDF-N stellar population: (left) K -band magnitude, (middle) $J - K$ color, and (right) X-ray luminosity. In each panel, histograms from top to bottom are: total stellar population in the CDF-N field with $V < 22.5$ without X-ray selection (thin solid line), *XCOUNT* model prediction with standard settings including X-ray selection and no $t > 1$ Gyr magnetic activity evolution (thin dashed line), *XCOUNT* model with rapid X-ray decay with $\alpha \times \beta = -2$ (thick dashed line), and the observed distributions (thick solid line).

Table 1. CDF-N 1 Ms sky coverage

Count rate (cts s ⁻¹)	Area (deg ²)
1.0×10^{-5}	0.0035
1.2×10^{-5}	0.0212
2.0×10^{-5}	0.0311
4.0×10^{-5}	0.0386
6.0×10^{-5}	0.0111
8.0×10^{-5}	0.0038
1.0×10^{-4}	0.0017
1.0×10^{-3}	0.0112

Note. — Count rates are in the 0.5–2 keV soft band.

Table 2. X-ray positions and counts of CDF-N stars

B01 #	Coordinates (error)		Off-axis '	Counts			Band Ratio	Ct Rate (ct Ms ⁻¹)	t_{eff} (ks)
	α_{2000}	δ_{2000} (")		FB	SB	HB			
<i>Statistical 1 Ms Sample</i>									
12	123536.14 + 621646.5	(1.2)	8.6	127 ± 20	130 ± 19	< 30	< 0.24	136	948
36	123555.13 + 621800.3	(0.9)	7.2	53 ± 14	53 ± 11	< 21	< 0.41	49	1073
53	123604.90 + 622013.9	(0.4)	7.9	382 ± 29	365 ± 29	< 41	< 0.12	418	871
106	123625.01 + 622115.7	(0.4)	7.7	224 ± 20	214 ± 17	< 25	< 0.12	204	1046
108	123625.39 + 621404.8	(0.3)	2.4	519 ± 25	478 ± 23	33 ± 8	0.07 ± 0.02	317	1509
128	123632.78 + 622027.2	(0.4)	6.7	396 ± 30	377 ± 29	< 29	< 0.08	237	1588
157	123640.12 + 621942.0	(0.7)	5.8	169 ± 17	166 ± 15	< 22	< 0.13	95	1741
302	123725.65 + 621649.0	(0.7)	5.5	97 ± 14	96 ± 12	< 20	< 0.22	52	1821
324	123737.99 + 621631.3	(0.9)	6.6	52 ± 14	49 ± 12	< 24	< 0.49	29	1671
341	123748.15 + 622126.8	(1.5)	10.4	195 ± 23	127 ± 16	79 ± 17	0.64 ± 0.16	139	917
370	123845.44 + 621002.5	(0.7)	14.5	218 ± 18	175 ± 15	34 ± 9	0.20 ± 0.06	4487	39
<i>Additional 2 Ms stars</i>									
...	123633.81 + 620807.7	(0.8)	6.0	38 ± 12	36 ± 9	< 22	< 0.63	20	1785
...	123652.95 + 620726.8	(0.9)	6.6	120 ± 18	110 ± 16	< 25	< 0.23	62	1763

Table 3. X-ray properties of CDF-N stars

B01 #	Spectrum						Var
	N_{H} (10^{21} cm^{-2})	kT_1 (keV)	kT_2 (keV)	χ^2_{ν} (ν)	f_{SB} ($10^{-16} \text{ erg s}^{-1} \text{ cm}^{-2}$)	f_{FB}	Num Flares
<i>Statistical 1 Ms sample</i>							
12	0.0	0.1	0.7 ^a	0.7 (10)	6	6	0
36	0.2	0.3	...	1.8 (4)	3	3	1
53	0.2	0.7	2.9	1.1 (13)	19	24	1
106	0.2	0.5	...	1.3 (17)	10	10	0
108	0.2	0.6	1.5	1.2 (32)	14	16	3
128	0.0	0.8	2.7	1.1 (11)	9	11	0
157	0.0	0.2 ^b	0.8	0.8 (11)	5	5	1
302	0.0	0.3	1.5	1.0 (8)	3	3	1
324	0.0	^c	1.7	1.8	0
341	0.2	...	2.2	0.8 (27)	6	9	0
370	0.0	0.1	1.4	1.3 (32)	205	261	1
<i>Additional 2 Ms stars</i>							
...	0.2	0.8	0.9	0.9	0
...	0.0	0.3 ^c	2.0	0.9 (11)	4	4	1

^aAn additional hard component with emission around 5 keV may be present.

^bAn additional ultra-soft component may be present.

^cNo good statistical fit was obtained for this weak source. Fluxes were derived by assuming $kT = 0.8 \text{ keV}$.

Table 4. Optical/IR properties of CDF-N stars

B01 #	Δ^a	B	V	R	I	J^b	H^b	K^b
<i>Statistical 1 Ms sample</i>								
12	0.6	17.59 ^c	12.60	12.06	11.92
36	0.5	22.50 ^c	21.25 ^d	20.15 ^c	17.79 ^d	16.23	15.81	15.22
53	0.5	20.82 ^c	19.58 ^c	18.19 ^e	...	15.41	14.66	14.48
106	0.2	...	14.53 ^d	13.27 ^e	13.56 ^d	11.35	10.88	10.79
108	0.2	20.37 ^c	19.25 ^d	...	16.65 ^d	15.17	14.55	14.23
128	0.1	...	17.94 ^d	...	16.22 ^d	14.77	14.13	13.91
157	0.5	18.80 ^c	16.57 ^d	...	15.07 ^d	12.87	12.24	12.01
302	0.5	22.12 ^c	21.09 ^d	20.05 ^c	18.03 ^d	15.8
324	0.4	...	14.02 ^d	13.12 ^e	13.08 ^d	10.70	10.26	10.19
341	1.8	24.09 ^c	19.62 ^d	...	17.07 ^d	15.76	15.30	15.21
370	0.3	14.17 ^c	12.45	12.14	12.06
<i>Additional 2 Ms stars</i>								
...	0.2	...	16.81 ^d	...	14.86 ^d	13.19	12.55	12.28
...	0.2	...	15.35 ^d	...	13.37 ^d	11.27	10.60	10.39

^aPositional offsets in arcseconds of the ACIS source with respect to the 2MASS Second Incremental Data Release (Cutri et al. 2000), except for source 302 where the optical source position was measured by Barger et al. (2003).

^bJHK magnitudes are from 2MASS except for source 302 where we use the HK' measurement of Barger et al. (2003) with the approximate conversion $K = HK' - 0.3$ (Barger et al. 1999).

^cFrom Barger et al. (2003).

^dMeasurement V and I plates of Wilson (2003).

^eMeasurement of R -band plate of Liu et al. (1999) but note that for sources #106 and #324, Liu's measurements were $R = 12.77$ and $R = 12.64$, respectively.

Table 5. Derived properties of CDF-N stars

B01 #	SpTy	Dis (pc)	$\log \frac{f_X}{f_K}$	$\log L_{SB}$ (erg s ⁻¹)
<i>Statistical 1 Ms sample</i>				
12	K4:	320	-3.51	27.7
36	M4	360	-2.46	27.5
53	M5	160	-1.97	27.8
106	K0	230	-3.72	27.7
108	M4	230	-2.23	27.9
128	M2	300	-2.53	28.1
157	M5	50	-3.55	26.1
302	M4	460	-2.28	27.8
324	G5:	220	-4.74	26.8
341	M4	360	-2.20	28.8
370	G8:	510	-1.91	29.8
<i>Additional 2 Ms stars</i>				
...	M4	90	-4.20	25.9
...	M2:	75	-4.35	26.2